AGU PUBLICATIONS

Journal of Advances in Modeling Earth Systems

RESEARCH ARTICLE
10.1002/2013MS000276

The effect of horizontal resolution on simulation quality in the Community Atmospheric Model, CAM5.1

Michael F. Wehner[1], Kevin A. Reed[2], Fuyu Li[1], Prabhat[1], Julio Bacmeister[2], Cheng-Ta Chen[3], Christopher Paciorek[4], Peter J. Gleckler[5], Kenneth R. Sperber[5], William D. Collins[1], Andrew Gettelman[2], and Christiane Jablonowski[6]

[1]Lawrence Berkeley National Laboratory, Berkeley, California, USA, [2]National Center for Atmospheric Research, Boulder, Colorado, USA, [3]Department of Earth Science and Institute of Marine Environmental Science and Technology, National Taiwan Normal University, Taipei, Taiwan, [4]Department of Statistics, University of California at Berkeley, Berkeley, California, USA, [5]Lawrence Livermore National Laboratory, Livermore, California, USA, [6]Department of Atmospheric, Oceanic, and Space Sciences, University of Michigan, Ann Arbor, Michigan, USA

Key Points:
- The effects of increasing resolution in an atmospheric model are presented
- Global models at 25 km can realistically simulate tropical cyclone statistics
- Increased resolution alone does not improve model defects

Correspondence to:
M. F. Wehner,
mfwehner@lbl.gov

Citation:
Wehner, M. F., K. A. Reed, F. Li, Prabhat, J. Bacmeister, C.-T. Chen, C. Paciorek, P. J. Gleckler, K. R. Sperber, W. D. Collins, A. Gettelman, and C. Jablonowski (2014), The effect of horizontal resolution on simulation quality in the Community Atmospheric Model, CAM5.1, *J. Adv. Model. Earth Syst.*, *6*, 980–997, doi:10.1002/2013MS000276.

Received 25 OCT 2013
Accepted 24 SEP 2014
Accepted article online 13 OCT 2014
Published online 5 NOV 2014

Abstract We present an analysis of version 5.1 of the Community Atmospheric Model (CAM5.1) at a high horizontal resolution. Intercomparison of this global model at approximately 0.25°, 1°, and 2° is presented for extreme daily precipitation as well as for a suite of seasonal mean fields. In general, extreme precipitation amounts are larger in high resolution than in lower-resolution configurations. In many but not all locations and/or seasons, extreme daily precipitation rates in the high-resolution configuration are higher and more realistic. The high-resolution configuration produces tropical cyclones up to category 5 on the Saffir-Simpson scale and a comparison to observations reveals both realistic and unrealistic model behavior. In the absence of extensive model tuning at high resolution, simulation of many of the mean fields analyzed in this study is degraded compared to the tuned lower-resolution public released version of the model.

1. Introduction

Confidence in projections of future climate change derived from global climate models is partly determined by their ability to simulate the observed recent past. In particular, the realistic simulation of intense storms is severely limited by the constraints on resolution typical of the global models used in national and international climate change assessments [*Melillo et al*., 2014; *Stocker et al*.., 2013], due to the fact that these storms are unresolved at even their largest scales. These limitations undermine confidence in projections of future changes in extreme precipitation and wind. Regional modeling studies may permit examination of some aspects of extreme weather, but may be adversely affected by the uncertainties in the lateral boundary conditions supplied by the coarser global models [*Duffy et al*., 2003]. For example, the global models that supplied the boundary conditions for the multiple regional models used the North American Regional Climate Change Project [*Mearns et al*., 2009] do not realistically simulate tropical storms due to inadequate resolution, nor do the domains of these regional models encompass the main Atlantic tropical cyclogenesis region. Thus, robust inferences about changes in extreme precipitation during the hurricane season in the Gulf Coast and Atlantic states of the U.S. are limited by systematic errors in the moisture flux at the boundaries of the regional domains. Also, by their very design, the limited spatial extent of regional simulations may complicate the robust detection and quantification of the controlling mechanisms for changes in extreme events. For these reasons, new global atmospheric models integrated for multiple decades at the resolutions of current regional models are a preferable framework for more realistic simulations of intense, localized storm characteristics, and more comprehensive statistical information about such events at the global scale.

Over the last decade, a growing number of studies have discussed the ability of high-resolution GCMs to simulate tropical storms. *Atlas et al*. [2005] and *Shen et al*. [2006a, 2006b] showed that the National Aeronautics and Space Administration (NASA) hydrostatic finite-volume GCM could adequately simulate tropical storms successfully at horizontal resolutions of 0.25° and 0.125°. *Oouchi et al*. [2006] used a global atmospheric model developed by the Meteorological Research Institute and Japan Meteorological Agency (MRI/JMA) at 20 km resolution to simulate the frequency, distribution, and intensity of tropical storms in the

current climate. Despite some limitations, the MRI/JMA model was able to generally reproduce the overall geographical distribution and frequency of tropical storms. Additional global model investigations include the studies by *Bengtsson et al*. [2007] and *Zhao et al*. [2009], who evaluated tropical storm climatological statistics in the Max-Planck Institute for Meteorology ECHAM5 model at the spectral resolution T319 (approximately 42 km) and in the Geophysical Fluid Dynamics Laboratory (GFDL) finite-volume cubed-sphere model [*Donner et al*., 2011] on a 0.5° grid, respectively. In addition, a version of the GFDL model has been used for the assessment of the interannual variability of tropical storms [*Chen and Lin*, 2011]. More recently, global cloud-resolving models, such as the Nonhydrostatic Icosahedral Atmospheric Model (NICAM) [*Tomita and Satoh*, 2004], have shown enhanced skill in the simulation of present and projected future tropical storm activity [*Fudeyasu et al*., 2008; *Yamada et al*., 2010]. At a similar model and resolution as evaluated here, *McClean et al*. [2011] demonstrated that a 0.25° atmosphere, 0.1° ocean version of CCSM4 demonstrated spontaneously generated category 4 cyclones that showed "realistic formation of a cold SST wake, mixed layer deepening, and warming below the mixed layer. Too many tropical storms formed in the North Pacific, however, due to too high SSTs in the tropical eastern Pacific. In the North Atlantic, anomalously low SSTs lead to a dearth of hurricanes." The latter results demonstrated the sensitivity of cyclone statistics to biases in SST.

This paper documents a 27 year simulation of the Community Atmospheric Model (version CAM5.1) at a resolution of approximately 28 km on the equator. This model, developed by the U.S. National Science Foundation and Department of Energy, joins a number of other global atmospheric general circulation models to be integrated at high resolution. Studies using a similar version of CAM5.1, including *Reed and Jablonowski* [2011b, 2012], have shown that the model is capable of simulating intense tropical cyclones at horizontal resolutions of 0.5° or less using an idealized vortex initialization technique [*Reed and Jablonowski*, 2011a]. Also, a previous version of CAM (version 2.2) was integrated at ∼50 km and used to study tropical storms [*Wehner et al*., 2010a] and the effect of resolution on very extreme U.S. precipitation return values [*Wehner et al*., 2010b]. As high-performance computing capabilities continue to evolve, other modeling groups will certainly join these high-resolution efforts.

In section 2 and Appendix A, we describe details of the model and its configuration in this simulation. Section 3 is a comparison of the high-resolution version of CAM5.1 to lower-resolution versions of the model in the context of available observations. We briefly discuss some computational aspects of both the simulation and the analysis of the large amount of model output in section 4. Finally, in section 5, we offer some general conclusions and discuss opportunities for future studies. Appendix A describes the differences in model input parameters between the CAM5.1 public release and those used in this study. Appendix B summarizes the global and basin-scale observed and simulated tropical storm statistics.

2. The High-Resolution Community Atmospheric Model CAM5.1

The model used in this study is the public release version of CAM5.1 available from http://www.earthsystemgrid.org. A complete description of the model dynamics and physical parameterizations, summarized in Appendix A, is more fully documented in *Neale et al*. [2010] and *Ghan et al*. [2012]. CAM5.1 forms one of the several atmospheric component options for the fully coupled Community Earth System Model (CESM), also available from the NCAR Earth System Grid web portal. It is an extraordinarily flexible modeling system that can be configured with a variety of possible combinations of dynamical cores and physics packages.

The performance of CAM5.1 is examined at three different horizontal resolutions using the finite-volume dynamical core on rectilinear latitude-longitude grids. The FV dynamical core is similar to that used in the tropical storm studies by *Atlas et al*. [2005], *Shen et al*. [2006a], and *Zhao et al*. [2009] but with different subgrid-scale physical parameterizations. In this study, model configurations at the different resolutions are held as close as possible to the others. The grids range from approximately 200 to 25 km in resolution. The coarsest mesh considered here is 1.9° in the latitudinal direction by 2.6° in the longitudinal direction. A 0.9° by 1.3° mesh is examined as an intermediate case. This intermediate resolution is the default NCAR-supported configuration and is as used in the CESM1.0 contributions to the Fifth Assessment Report (AR5) of the Intergovernmental Panel on Climate Change. This paper is complementary to a recent study of high-resolution versions of CAM4 and CAM5 by *Bacmeister et al*. [2013], which concluded that large-scale mean seasonal aspects of the simulated climate are not dramatically improved by the increase in resolution. This

paper extends the analysis of seasonal mean climate to more variables. However, our principal motivation here is to explore the effect of resolution on simulated extreme precipitation and on simulated tropical storm climatology. We note that the configuration of CAM5.1 is the same in the two studies.

The finest resolution considered in this study is based on a mesh of 0.23° by 0.31°. This resolution is still well suited to the hydrostatic approximation of the finite-volume dynamical core. However, it pushes the limits of the subgrid-scale parameterizations, particularly current representations of cumulus convective processes [*Arakawa and Wu*, 2013]. All three configurations in this study employ a standard 30 vertical level (L30) spacing scheme with a model top at approximately 2 hPa [*Reed and Jablonowski*, 2012]. Differences among select parameters employed for the three resolutions required by tuning and stability considerations are listed in Table A1 of Appendix A.

Surface forcing of the atmospheric model is accomplished through prescribed sea surface temperatures and sea ice extent that follow the protocols of the Atmospheric Model Intercomparison Project (AMIP) [*Gates*, 1992; *Gates et al*., 1999]. These lower boundary conditions are available as part of the CESM public release. The integration and analysis period spans 1979–2005. At least one full year of integration was performed as a spin-up prior to this period and discarded for each resolution. In addition, the well-mixed greenhouse gases and both tropospheric and stratospheric ozone vary from year to year [*Neale et al*., 2010]. The aerosol forcing is also prescribed through external inputs since the default prognostic aerosol package was disabled in the interests of computational efficiency. This prescribed bulk aerosol formulation is as in CAM4 and designed to interact with the CAM5 cloud physics following *Gettelman et al*. [2008], adjusting sulfate activation so that drop number concentrations are similar to standard CAM5.1. All input forcing field files are available in the public release.

The controlled experimental setup described above permits an assessment of the effects on model output of increased horizontal resolution with minimal changes to the details of the parameterizations. However, as detailed in *Bacmeister et al*. [2013], simply increasing horizontal resolution does not substantially improve large-scale measures of the simulated mean climatology. In fact, poor model performance that is caused by inaccurate or incomplete physical parameterizations may be exacerbated by changing resolutions. Systematic improvements are confined to aspects of the simulated climatology dependent on moving features from unresolved to resolved scales. For instance, more realistic topography at high resolution does drive significant local changes near mountainous regions sometimes resulting in improvements in the mean climatology downstream from them. Higher resolution is shown in section 3 to permit more intense storms in all regions resulting in improvements in extreme precipitation in some seasons and locations. Physically plausible simulations of tropical storms have been demonstrated using climate models at high resolution and have been analyzed to study changes in their statistical behavior as the climate warms [*Yoshimura and Sugi*, 2005; *Oouchi et al*., 2006; *Zhao et al*., 2009; *Sugi et al*., 2009; *Yamada et al*., 2010; *Knutson et al*., 2010; *Strachan et al*., 2013]. However, systematic improvements are not guaranteed, as the effects of resolution alone may not ameliorate biases in large-scale fields that affect storm locations and intensities [*Boyle and Klein*, 2010].

We refer readers interested in the detailed effect of resolution changes to the simulated climatology in CAM to *Bacmeister et al*. [2013]. However, to put changes in extreme precipitation in context, we briefly review mean precipitation in CAM5.1 at different horizontal resolutions. Like its previous versions, the tuned, publically distributed 0.9° × 1.3° version of CAM5.1, exhibits a spurious "double ITCZ" pattern in the Pacific. In the GPCP observations, the Intertropical Convergence Zone (ITCZ) exhibits both a band of enhanced precipitation slightly north of the equator and the South Pacific Convergence Zone (SPCZ) extending from the maritime continent toward the southeast. As is typical in global atmospheric models with this defect, the SPCZ simulated in CAM5.1 extends too far to the east. The double ITCZ is evident in Figures 1b–1d as two local maxima in the eastern tropical Pacific when considering a north to south cross section. Furthermore, simulated precipitation is too high in the eastern tropical Pacific and too low in the western tropical Pacific. These ITCZ errors are not improved in the high-resolution configuration of CAM5.1 illustrating that the source of the errors is likely not simply inadequate resolution but rather a deficiency in the underlying physical parameterizations. Such errors may be influenced by the lack of energy budget tuning (due to high computational costs) of the high-resolution configuration. However, given that there are many similarities in the error structure at all three resolutions examined here, it seems unlikely that radiation balance errors in the high-resolution version are the principal source of the precipitation bias.

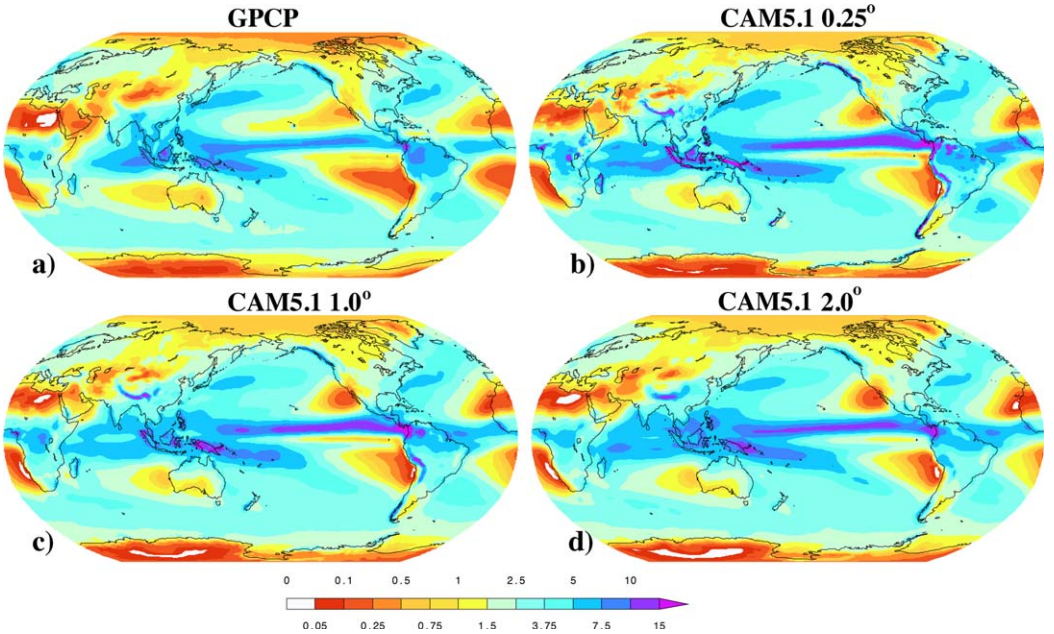

Figure 1. The 1979–2005 annual mean precipitation for the GPCP observations and the three different CAM5.1 resolutions. (a) Observations, (b) CAM5.1 0.23° × 0.31°, (c) CAM5.1 0.9° × 1.3°, and (d) CAM5.1 1.9° × 2.6°. All results are shown at the native resolution. Units: mm/d.

3. Model Performance

3.1. Extreme Precipitation Climatology

3.1.1. Precipitation Distribution

The distribution of daily precipitation is generally projected to shift toward more heavy precipitation days and fewer low-precipitation days as the climate warms [*Karl et al*., 2009; *Seneviratne et al*., 2012]. Accurate simulation of the observed precipitation distribution is critical to placing high confidence in such projected future changes. The probability density distributions of the observed and simulated precipitation are depicted in Figure 2 averaged over a variety of regions for the three model configurations and available gridded observed daily precipitation products.

Six different regions are considered in our analysis of extreme precipitation as dictated by the availability of seven different daily precipitation observational data sets. The six regions are (a) global land and ocean, (b) global land only, (c) tropical land and ocean, (d) contiguous U.S. (CONUS), (e) Asia, and (f) Europe. Two satellite products and four products derived from weather station data are used in this evaluation of model performance. The first satellite product is the Global Precipitation Climatology Project (GPCP) 1° × 1° daily precipitation product, version 1DD V1.1 [*Huffman et al*., 2001; *Bolvin et al*., 2009], covering all global land and ocean points, The second is the 3B42 daily TRMM-adjusted merged-infrared (IR) precipitation product from the Tropical Rainfall Measuring Mission (TRMM) [*Huffman et al*., 2007] and covering land and ocean points from 50°S to 50°N. The station data products are (1) the global data set of the Surface Water Modeling group at the University of Washington (UW-Global) [*Adam and Lettenmaier*, 2003; *Maurer et al*., 2009], the Daily U.S. Unified Precipitation product from the NOAA Climate Prediction Center (CPC) [*Higgins et al*., 2000], the CONUS data set of the Surface Water Modeling group at the University of Washington (UW-CONUS) [*Maurer et al*., 2002], the APHRODITE Project: Asian Precipitation—Highly Resolved Observational Data Integration Toward Evaluation of Water Resources [*Yatagai et al*., 2012], and the ENSEMBLE Project: E-Obs [*Haylock et al*., 2008].

There are variations between the different observed distributions when they are available over the same regions. There is little guidance in the literature as to which of the observational products is superior. Hence, we interpret these differences as a crude measure of observational uncertainty as in *Covey et al*. [2002] and plot the observations in Figure 2 as an envelope encompassing the minimum and maximum values reported. A comprehensive discussion of observational uncertainty would include satellite retrieval

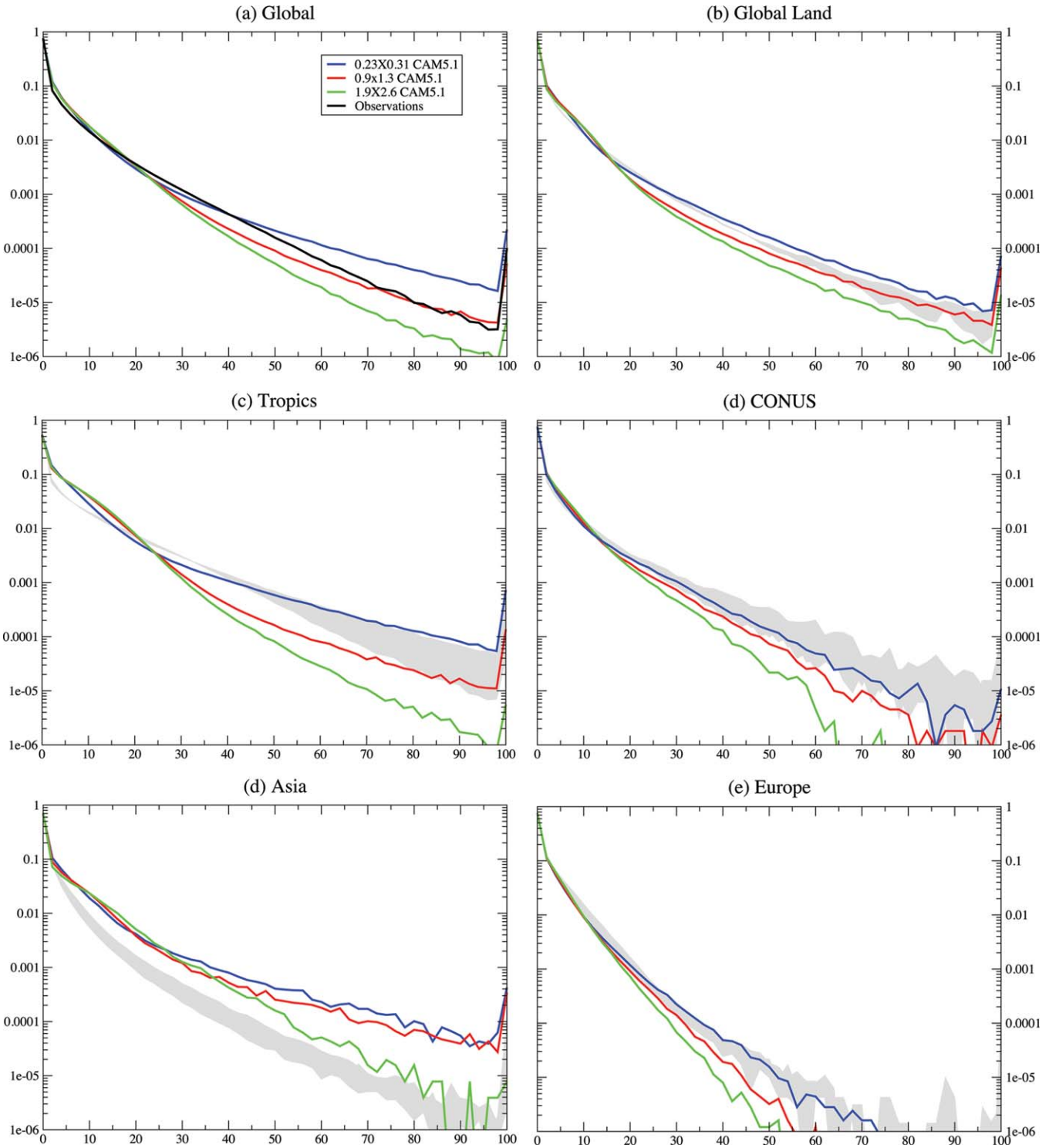

Figure 2. Comparisons of the annual probability density distributions of daily precipitation (mm) between the models and location-specific gridded observations as indicated by the data set name in parentheses. (a) Global land and ocean, (b) global land only, (c) tropical land and ocean, 20°S–20°N, (d) CONUS, (e) Asia (as covered by APHRODITE), and (f) Europe (as covered by E-OBS). Red, blue, and green, respectively, represent the 1.9° × 2.6° CAM5.1, 0.9° × 1.3° CAM5.1, and 0.23° × 0.31° CAM5.1 models. Observations are represented by the black line in Figure 2a and by gray shading in Figures 2b–2f, indicating the range of available data sets. Daily precipitation was remapped onto the 1.9° × 2.6° grid before computing the distributions in all cases.

algorithms as well as the sparseness of station data in many parts of the world but is outside the scope of this paper. In Figure 2, both model output and observations have been regridded onto the coarse 1.9° × 2.6° model grid before calculating these distributions. Daily accumulated precipitation over the entire

region of interest is aggregated into 2 mm/d bins from 0 to 100 mm/d. Any precipitation rates larger than 100 mm/d are assigned to the last bin for normalization purposes that sometimes results in an uptick at the end of the plot.

Figure 2a shows the probability density distributions of the models and the GPCP observation averaged over all global points, both ocean and land. All three versions of the model agree well with the GPCP distribution (shown in black) below 30 mm/d. Consistent with earlier studies [e.g., *Boyle and Klein*, 2010; *Li et al*., 2011], we find that increased model horizontal resolution results in increased heavy rainfall even after regridding to the coarsest model resolution. The 1.9° × 2.6° model simulation (shown in green) overestimates light precipitation (excessive drizzle) and underestimates the heavy precipitation. The 0.9° × 1.3° model simulation (shown in red) agrees well with these observations, but extreme precipitation in the 0.23° × 0.31° model simulation (shown in blue) is more frequent than in the GPCP observations. The heaviest daily precipitation events are in the ITCZ and it is in this region that the extreme value differences between the high-resolution simulation and the GPCP observations are the largest.

Figure 2b shows the probability density distributions of the models and the range of UW-Global and GPCP data sets averaged over all global land points. The station data distribution lies above the satellite estimate above 50 mm/d. The range of observations in Figures 2b–2f are shown by the gray envelope. In this comparison, the models start to diverge from each other and the observation at precipitation rates greater than 20 mm/d. The 1.9° × 2.6° model is below the range observations thereafter. The 0.9° × 1.3° model is below the range of observations between 20 and 60 mm/d but follows the range of observations thereafter. The 0.23° × 0.31° model slightly exceeds the range of observations above 30 mm/d.

Figure 2c shows the probability density distribution of the models and the range of the TRMM and GPCP data sets averaged over all tropical (20°S–20°N) land and ocean points. In this comparison, the models overestimate the frequency of tropical precipitation rates lower than 20 mm/d. TRMM provides a significantly higher estimate of extreme precipitation occurrence in the tropics than does GPCP above 40 mm/d. The 0.23° × 0.31° model simulation is slightly higher than the range of observations in this comparison at rates greater than 30 mm/d. The other two model distributions are significantly lower than observed for extreme precipitation rates in the tropics.

Figure 2d shows the probability density distribution of the models and the range of the UW-CONUS, UW-Global, CPC, TRMM, and GPCP data sets averaged over the contiguous U.S. Over the CONUS region, the GPCP provides the lower bound while TRMM provides the upper bound of the observational range over most values of precipitation rates. The station-based products lie in the middle of the range for precipitation rates greater than 30 mm/d. The U.S. and Europe regions have the highest station density on the planet, so confidence in the observational range is higher than for the global and semiglobal regions shown in Figures 2a–2c. In this comparison, the models' distributions agree well with the observation below 20 mm/d. The 1.9° × 2.6° model distribution is undersampled above 60 mm/d indicating that either such extreme precipitation rates are rare events in a simulation of this length or are near the maximum precipitation rate permitted at this resolution. The 0.23° × 0.31° model's distribution is undersampled above 80 mm/d when remapped to the 1.9° × 2.6° grid but clearly agrees with the observation better than the 0.9° × 1.3° model in this comparison.

Figure 2e shows the probability density distribution of the models and the range of the UW-Global, APHRODITE, and GPCP data sets averaged over most of Asia. This comparison differs substantially from the others in that all three model configurations produce results significantly higher than the observational range. We attribute this to the large dry areas in the region covered by the APHRODITE region influencing the normalization of the probability density distribution and that the models all produce roughly the observed total amount of precipitation over the region. However, the difference between simulated distributions and the observations becomes apparent in the second bin of precipitation rates (2–4 mm/d) which exceeds the annual mean value in the vast dry parts of Northern Asia. When subsampling the region to include only India or eastern China, the tail of the higher-resolution simulated distributions are higher than the lower-resolution simulated distributions and are closer to the observations, similar to the CONUS results. We return to this point below.

Figure 2f shows the probability density distribution of the models and the range of the UW-Global, E-OBS, and GPCP data sets averaged over most of Europe. In this comparison, the observation is undersampled

above 60 mm/d when remapped to the 1.9° × 2.6° grid and limited to the 1979–2005 period. Over the European region, the E-Obs station data lie below the satellite GPCP estimate, in contrast to the relative magnitudes over the CONUS region. The models' distributions agree well with the observations at precipitation rates <20 mm/d. At greater rates, the range of observations lies above the 1.9° × 2.6° and the 0.9° × 1.3° models. However, similar to the CONUS region, the 0.23° × 0.31° model lies within the observational range in Europe.

While the interpretation of which model configuration is superior may seem contradictory from the results presented in Figure 2, the unquantified observational uncertainties must be considered. Clearly, across the globe, higher precipitation rates are permitted by the high-resolution model than by the lower-resolution configurations. In some cases, this precipitation rate may indeed be too high. However, in the two regions which are most well observed, Europe and CONUS, the daily precipitation distribution function of the 0.23° × 0.31° configuration lies within the range of observations while the lower-resolution configurations do not.

3.1.2. Measures of Extreme Precipitation

In this section, we consider two different metrics to assess the effect of model resolution on extreme precipitation patterns and magnitudes. The first is a measure of longer duration extreme precipitation; the annual maximum 5 day accumulated precipitation commonly referred to as *Rx5day* [*Frich et al*., 2002; *Alexander et al*., 2006]. The second metric is the 20 year return value of the seasonal maximum daily precipitation. This measure describes much rarer and shorter duration events than *Rx5day* and can be thought of as being farther down the right-hand tail of the distributions shown in Figure 2. Also, we maintain seasonality in the return value calculations as precipitation statistics vary between seasons due to the underlying larger-scale meteorological causes of extreme precipitation. Extreme precipitation statistics from the two lower-resolution configurations used in Figures 2–4 below were chosen at random from a single realization of the 50 member ensembles.

Figure 3 shows the mean value of *Rx5day* calculated from the 0.5° UW-Global station-based gridded data [*Adam and Lettenmaier*, 2003; *Maurer et al*., 2009] and the three CAM5.1 grid configurations over land points calculated on their native grids. Observations are calculated from the period 1979 to 1999. Model results are calculated from the period 1979 to 2005. As in our previous study [*Wehner et al*., 2010b], higher-resolution versions of the model produce larger extreme precipitation rates. Over regions where the gridded observations are well constrained by station gauge measurements, agreement between the observations is qualitatively better with the 0.23° × 0.31° version of the model. *Rx5day* is shown in Figure 3 as a mean daily precipitation rate with units of mm/d to facilitate comparison with other precipitation figures in this study. We made quantitative comparisons (not shown) of simulated and observed estimates of *Rx5day* over land points in two ways. The first was to compare model and observed *Rx5day* calculated from daily precipitation rates regridded to the 1.9° × 2.6° grid. The second was to regrid the high-resolution daily observations (CPC, UW-CONUS, APHRODITE, and E-Obs) to the native model grids prior to the calculation of *Rx5day*. As the UW-Global observations are coarser than the 0.23° × 0.31° model configuration, we performed the second comparison on the UW-Global native mesh instead in this case. Comparison on the native grids preserves whatever fine-scale structure the model can reproduce. From a certain viewpoint, this comparison may be more relevant for the evaluation of the models' precipitation extremes as the ability to simulate large values is so critical to interpreting the impacts of projected future changes. However, we found that for *Rx5day* both methods produced essentially the same Root Mean Square Error (RMSE) and skill scores as measured on a Taylor plot [*Taylor*, 2001]. Compared against the UW-Global data, the 0.23° × 0.31° model configuration scores essentially the same skill (∼0.75) as the 0.9° × 1.3° model configuration. A analogous comparison of the coarsened models against the GHCNDEX global estimate of *Rx5day* [*Donat et al*., 2013] reveals similar behavior. Over the CONUS region, the 0.23° × 0.31° model configuration scores significantly higher Taylor skill (>0.9) than the 0.9° × 1.3° model configuration (∼0.8) when compared against either the UW-CONUS or CPC observations. The skill score differences between these two model configurations compared to Asian (APHRODITE) and European (E-Obs) observations are minor. The 1.9° × 2.6° model configuration consistently scores the lowest over all regions.

In a stationary climate, the 20 year return value is that value expected to be exceeded on average once every 20 years over a long period of time. However, both the observed climate and the simulated climate in this study are changing. In a changing climate, the annual (seasonal) 20 year return value is interpreted as that value that has a 5% chance of being exceeded over the course of a given year (season). Because the

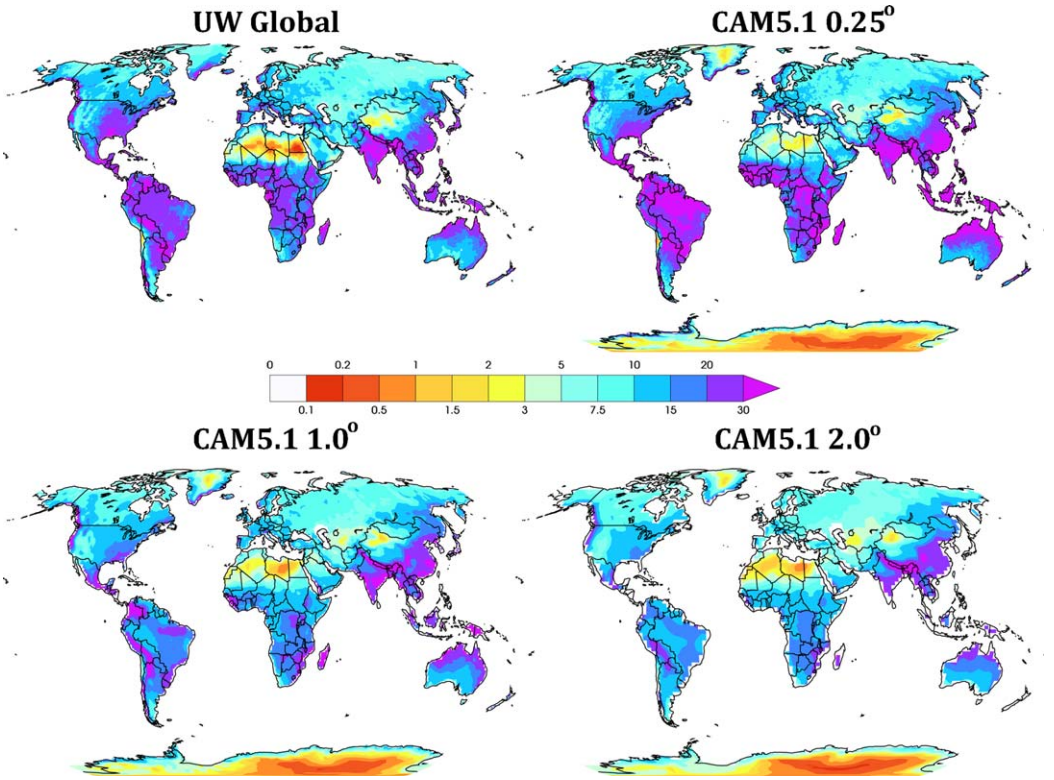

Figure 3. Simulated and observed annual maximum 5 day accumulated precipitation over land points, *Rx5day*, averaged. Observations are calculated from the period 1979 to 1999. Model results are calculated from the period 1979 to 2005. All results are shown at the native resolution. (a) 0.5° UW-Global gridded observations, (b) 0.23° × 0.31° CAM5.1, (c) 0.9° × 1.3° CAM5.1, and (d) 1.9° × 2.6° CAM5.1. Units: mm/d.

tail of the distribution of daily precipitation is generally well behaved [*Coles*, 2001], extreme value statistical techniques are well suited to estimate such long period return values. Figure 4 shows the 20 year return values of the winter and summer maximum daily precipitation from the 0.5° UW-Global station-based gridded

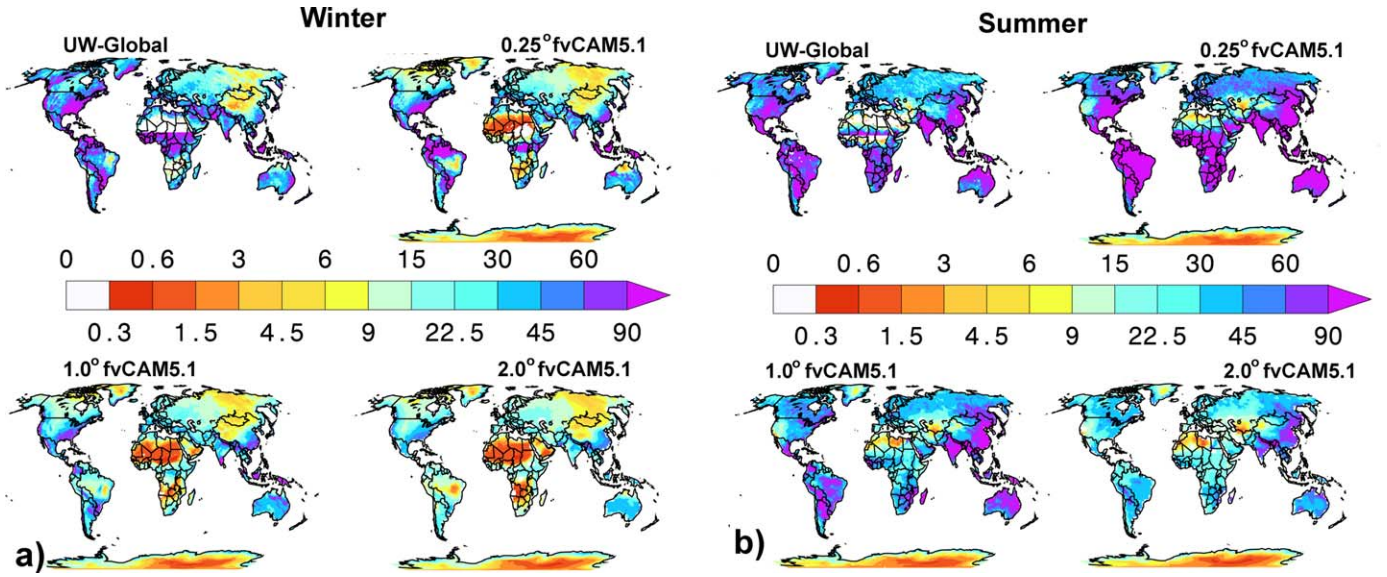

Figure 4. Simulated and observed values of the 20 year return values of the seasonal maximum daily precipitation over land. Observations are calculated from the period 1979 to 1999. Model results are calculated from the period 1979 to 2005. All results are shown on the native grids. (a) Winter. (b) Summer, 0.5°. Units: mm/d.

data [*Adam and Lettenmaier*, 2003; *Maurer et al*., 2009] and the three CAM5.1 grid configurations over land points calculated on their native grids using a time-dependent statistical extreme value formulation, in particular the point process approach to analyzing peaks over a high threshold [*Coles*, 2001]. In our analysis, the location parameter is fit to a linear function of time while the shape and scale factors are fit to constants. We analyzed all daily precipitation values exceeding a threshold set to the 95th percentile (calculated separately for each location and season) of all daily precipitation values exceeding 0.1 mm/d. Observations are calculated from the period 1979 to 1999. Model results are calculated from the period 1979 to 2005. Figure 4 shows the time-dependent return values evaluated at the midpoint of the time series. The seasons are defined appropriately to each hemisphere, i.e., winter is the December-January-February average in the north and the June-July-August average in the south. Extreme value distributions have been demonstrated many times to be a suitable function to describe the far tails of both simulated and observed precipitation based on the Kolmogorov-Smirnov goodness-of-fit test [*Kharin et al*., 2007, 2013] and the Anderson-Darling goodness-of-fit test [*Wehner*, 2012]. As a result, standard errors in these estimates of return values resulting from both the fitting method and sample size are negligible compared to the differences between model configurations and observations.

As found in an earlier version of the CAM [*Wehner et al*., 2010b], Figure 4 reveals that simulated precipitation return values increase with increased horizontal model resolution at all locations and all seasons without an indication of convergence. Comparison of the simulated to the observed return values reveals reasonably improved agreement as resolution increases. For instance, over most of the Northern Hemisphere winter, the highest resolution appears to agree better with the observations than the two lower resolutions. Although not shown, similar agreement is shown in the shoulder seasons. However, this is not the case for eastern China and monsoon season India where the high-resolution model produces very extreme precipitation values that are too large. In the Southern Hemisphere, agreement is better in the winter than in the shoulder seasons but many regions are poorly constrained in these gridded observations. In the summer season, simulated values in the high-resolution model configuration are much larger than observed over most of the globe. Consistent with most of the regional models in the North American Regional Climate Change Assessment Program (NARCCAP) [*Wehner*, 2012], the high-resolution CAM5.1 generally predicts excess extreme precipitation in the wet, warm regions, or seasons. We hypothesize that the source of this common error may be the interaction of the cumulus and large-scale precipitation parameterizations in situations when specific humidity is large and near saturation. Our specific hypothesis is that a mismatch of the 1 h relaxation time scale in CAM5.1 Zhang-McFarlane-based cumulus parameterization and the 15 min physics time step (Table A1) is overstabilizing the atmosphere thus permitting fully saturated conditions too frequently. This mismatch of time scales is doubled over that in the low-resolution configurations (with their 30 min time steps). Previous studies [*Li et al*., 2011] reveal that the contribution to daily precipitation rates from the cumulus parameterization in CAM does not exceed about 30 mm/d. In the summer, the large precipitation rates from the high-resolution model shown in Figure 4b must then be produced by the large-scale precipitation parameterization. The mismatch of time scales implies that the adjustments to temperature and moisture from the cumulus package are too frequent given the assumptions in the Zhang-McFarlane scheme. One possibility is that the net effect of the temporal mismatch is to reduce the amount of moisture removed from a model column by cumulus processes allowing large saturations to build up which eventually are removed by the large-scale precipitation parameterization. However, additional numerical experiments are necessary to fully test this hypothesis as other sources of this error during warm periods are quite possible.

The differences in the quality of the agreement of the models' seasonal return values with the available observations were quantified over land (not shown) by the two methods detailed above for *Rx5day*. Unlike our evaluation of *Rx5day* where the two methods produced essentially the same results, the comparison of seasonal return values on the coarse grid produced smaller values of RMSE and larger skill scores than the comparison on native grids. This effect was larger on the $0.23^\circ \times 0.31^\circ$ model configuration than on the $0.9^\circ \times 1.3^\circ$ model configuration leading to different conclusions as to which is the superior model in some cases. Summer return values in the high-resolution model are consistently too high as they also are for all seasons in the tropics. However, the high-resolution model's return values are generally superior in the winter and spring seasons to the lower-resolution configurations in the nontropical regions. Both lower-resolution models generally produce precipitation return values significantly lower than the observational products in a seasons and regions. Hence, our evaluation can produce similar RMSE and skill scores even

though the error structure is very different between model configurations. As was the case in the evaluation of *Rx5day*, the 1.9° × 2.6° model configuration consistently scores the lowest.

Compared to the UW-Global observations, the Taylor skill of the 0.9° × 1.3° model configuration is higher than the 0.23° × 0.31° model configuration when evaluated on native grids. Over the CONUS and Europe, the highest resolution model scores better than the public release model in the winter and spring, but scores worse over Asia when evaluated on the native grids. However, when evaluated on the coarse grid, the high-resolution model scores considerably higher both globally and regionally in all seasons. As a result, the 0.23° × 0.31° model configuration scores the same or better in all comparisons of seasonal return value than the 0.9° × 1.3° model configuration when evaluated on the coarse grid.

A simple summary of our Taylor plot analyses (not shown) is to consider how the distribution of skill changes with resolution. We performed 44 different evaluations of *Rx5day* and seasonal return values across the regions defined in Figure 2. When comparing on native grids, the number of comparisons with Taylor skill greater than 0.75 is 2 for the 1.9° × 2.6° configuration, 8 for the 0.9° × 1.3° configuration, and 13 for the 0.23° × 0.31° configuration. Conversely, the number of comparisons with a modified Taylor skill <0.5 is 18 for the 1.9° × 2.6° configuration, 3 for the 0.9° × 1.3° configuration, and 12 for the 0.23° × 0.31° configuration. Both the highest and lowest skill values of the extreme precipitation measures are found in the high-resolution version of the model corresponding to the improvement in winter/spring and degradation in summer. A similar analysis of Taylor skills on the coarse grid reinforces our conclusion about high scores, with a few exceeding 0.9 for the high-resolution model. We note that no such dramatic shifts with changing resolution are found in our analysis of the models' skill in simulating mean fields where the majority of skill values exceed 0.95 for all three model configurations.

When cumulus processes do not play a significant role in simulated storms, the high-resolution model generally produces more realistic extreme precipitation. However, it is clear from Figures 2–4 that convergence of extreme precipitation in CAM5.1, even when analyses are performed on the coarsest grids, has not occurred in many regions, especially when they are warm and wet. In order to more accurately quantify model performance in the simulation of extreme precipitation, an assessment of the relative merits of the observed data sets used in this study as well as from other sources should be made by the international community. An "expert guidance" document would be invaluable in this regard.

3.2. Tropical Cyclones

One of the principal motivations for high-resolution global climate models is to study the statistical behavior of tropical cyclones. Models that permit the formation of such storms can be used to explore how these statistics may change as the global climate changes [*Oouchi et al*., 2006; *Bengtsson et al*., 2007; *Zhao et al*., 2009]. Comparisons of such models with observations then focuses not on specific storm tracks but on the statistical behavior of a large number of storms and their general physical characteristics. The interannual variability of tropical storm statistics is partially controlled by the patterns and magnitude of seasonal sea surface temperatures (SST), especially at the basin scale. For example, the El Nino/Southern Oscillation (ENSO) affects tropical storm statistics, but other modes of climate variability may also affect tropical storm statistics [*Camargo et al*., 2010; *Camargo and Sobel*, 2010]. Factors other than SST also play a role in the interannual variability of tropical storms necessitating fairly long comparison periods to ascertain model quality with confidence.

To quantify model produced tropical storm statistics, we use the tracking algorithm from the Geophysical Fluid Dynamics Laboratory (GFDL) with the threshold values for vorticity, warm core temperature anomaly, and planetary boundary layer depth as in *Knutson et al*. [2007]. We have ported this algorithm to massively parallel computing systems, exploiting the embarrassingly parallel time dimension [*Prabhat et al*., 2012], and incorporated additional diagnostics related to the spatial extent of tracked storms. Identification of weak simulated tropical storms is sensitive to these thresholds. Similarly, the classification of weak actual tropical storms is known to be nonuniform in time as observation technologies have improved [*Landsea et al*., 2010].

Over the period 1979–2005, the tracking algorithm identified 2231 cyclones of tropical storm strength or greater (∼83/yr) in the 0.23° × 0.31° CAM5.1 simulation. To approximate the instantaneous wind speed at a height of 10 m from the prognostic velocity components at lowest model level, the following power law is used,

$$u_{10} = (10.0/h)^{0.11} u_{lowest} \quad (1)$$

where $h \sim 50$ m is the approximate depth of the lowest model level and u_{lowest} is the speed at that level. This version of the model produced tropical storms up to category 5 on the Saffir-Simpson scale with some of them exhibiting a central precipitation minimum characteristic of the "eye of the storm." The tracking algorithm identified 239 events of tropical storm strength or greater (~8.9 per year) over this period in the 0.9° × 1.3° CAM5.1 simulation with the strongest storms at the category 3 level. No tropical storms at all were identified in the 1.9° × 2.6° version using the standard threshold values of *Knutson et al*. [2007].

Table B1 in Appendix B shows the annually averaged number of storms identified as tropical storm, tropical cyclone (category 1 or greater), and intense tropical cyclone strengths (categories 4 and 5) produced by 0.23° × 0.31° CAM5.1 over the period 1979–2005 for the entire globe and the Atlantic, Pacific, and Indian Ocean basins compared to observations data set. These observations are a combination of data from NOAA's Tropical Prediction Center for the North Atlantic and East Pacific and from the U.S. Navy's Joint Typhoon Warning Center for all other ocean basins. The combined data set was downloaded from: ftp://texmex.mit.edu/pub/emanuel/HURR/tracks/. While there is no formal citation to this data set, the bias corrections are described in Appendix of *Emanuel* [2007] and the online supplement of *Emanuel* [2005]. Hence, we subsequently refer to this data set as the "Emanuel tracks." Storm duration is also compared in Table B1 between the models and observations. Similar results were found when compared to the International Best Track Archive for Climate Stewardship (IBTrACS) observed track database [*Knapp et al*., 2010]. The basin boundaries are given in Table B2.

Figure 5 shows the global storm tracks identified in the 1979–2005 integration of 0.23° × 0.31° CAM5.1 compared to the observed Emanuel tracks. Storms are colored according to their strength on the Saffir-Simpson scale. While agreement at the global scale is reasonable, examination at basin scales or finer reveals some systematic biases. From Table B1, the total number of simulated tropical cyclone strength storms in the Pacific agrees well with observations, but the partition between the eastern and western portions of the basin is reversed. As a result, there is a tendency for more simulated storms in the central tropical Pacific than is observed. Also, the model is overactive in the North Indian Ocean, in particular in the Arabian Sea. The total number of simulated Atlantic storms agrees well with observations across the range of intensities from tropical storms to intense tropical cyclones. The partition of Atlantic tropical cyclogenesis between the eastern Atlantic and the Caribbean roughly matches the observations. However, for CAM5.1 many storms in the Atlantic originate closer to the coast of Africa than they do in the observations leading to a higher density of storm tracks in the middle of the basin than is observed. These biases are also evident in maps of observed and simulated storm track density (not shown here but similar to Figure 12 of *Bacmeister et al*. [2013]).

The simulated number of tropical storm days is much larger in the high-resolution simulation than observed. As the number of simulated tropical storms is about the same as observed, the average duration of simulated tropical storms is too long compared to the observational record. While this may be due in part to a more complete knowledge of the simulated storms' wind speeds at all grid point locations at all times that is not possible with observations of actual storms, a tendency to maintain simulated tropical storm intensities for longer than they should be is likely a significant model bias. The global model errors in both storm days and counts are largest (and positive) for weak tropical storms and slightly negative for intense tropical cyclones as seen in Table B1.

Simulated and observed monthly tropical cyclogenesis climatology are shown in Figure 6. Results are only shown for the high-resolution (0.23° × 0.31°) version of CAM5.1. The strong seasonal cycle in the North Atlantic is well reproduced in the high-resolution simulation indicating that the simulated wind shear responds adequately to the seasonal SST variations in that basin. The complex observed cyclogenesis seasonality in the Indian Ocean is partially simulated. The model does produce the correct local maximum in May and June relative to the previous and succeeding months but is weak and a month late in simulating the peak centered in October and November. In the West Pacific, the model is underactive relative to the observations but simulates the seasonality well. This is because the storms are originating more in the Central/East Pacific as described earlier. In the East Pacific, the model is starts the tropical storm season too early and terminates too late resulting in a season 3–4 months too long.

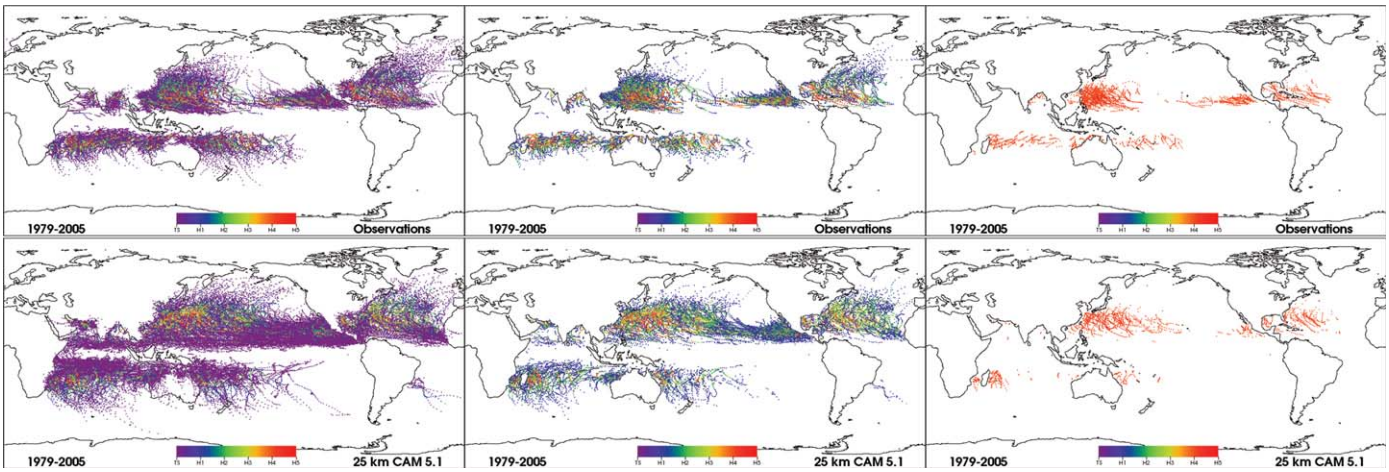

Figure 5. Tropical storm tracks identified by the GFDL tracking algorithm in the 1979–2005 integration of (bottom row) the 0.23° × 0.31° CAM5.1 and (top row) the Emanuel tracks. Colors indicate maximum wind speeds on Saffir-Simpson scale. (left column) Tropical storm strength and larger. (middle column) Tropical cyclone strength and larger. (right column) Intense tropical cyclone strength

Observed and simulated interannual variations of the number of tropical storms are shown for these four Northern Hemisphere basins in Figure 7. Results are only shown for the high-resolution (0.23° × 0.31°) version of CAM5.1. Correlations between the observed and simulated storm counts are generally low for all basins. However, there are periods when the simulated storm counts are reasonably correlated with observed counts.

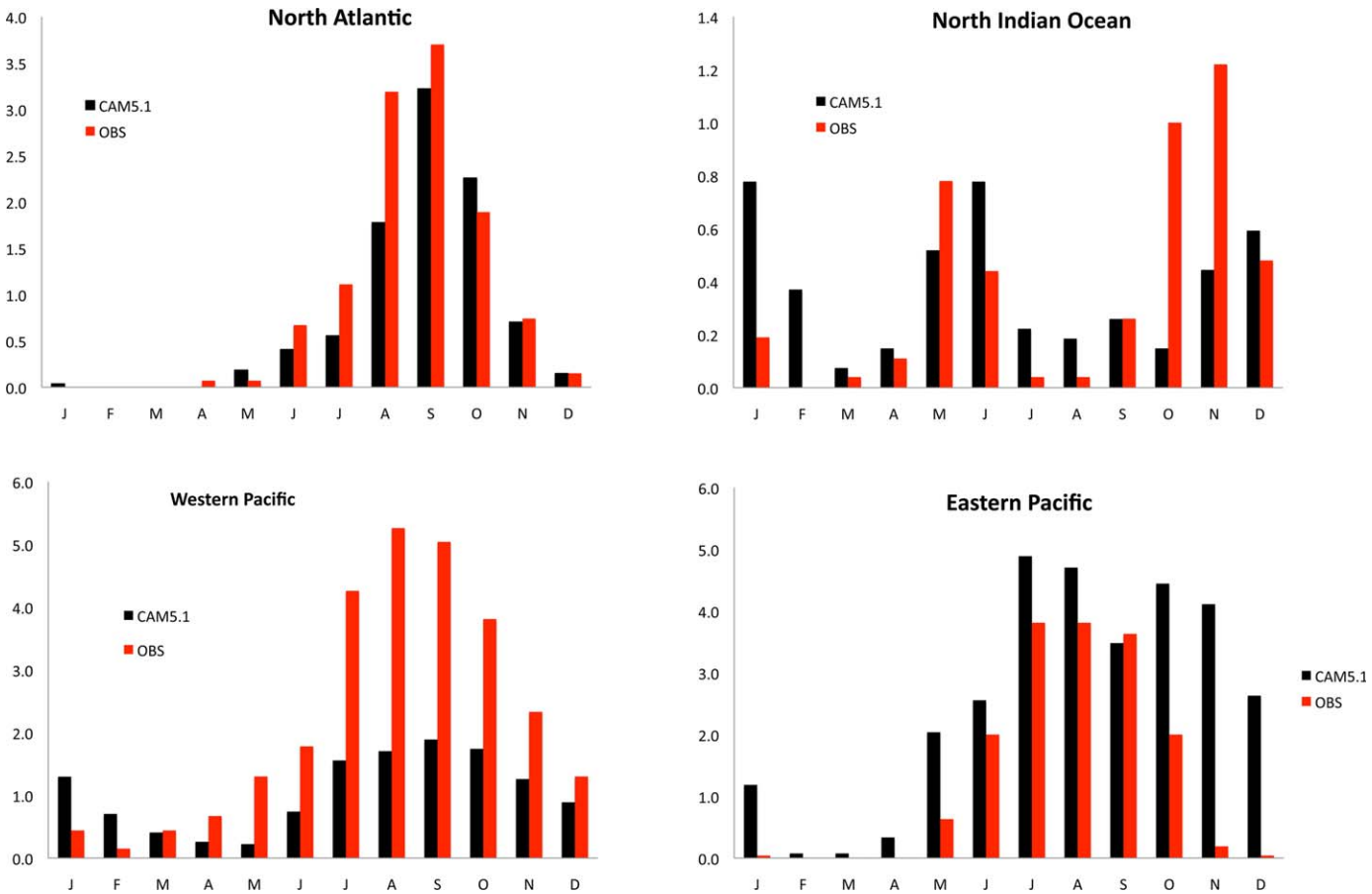

Figure 6. Monthly climatology of simulated (black) and observed (red) tropical storms averaged over 1979–2005 in selected Northern Hemisphere ocean basins for the high-resolution CAM5.1. (top right) North Atlantic. (top left) North Indian. (bottom left) West Pacific. (bottom right) East Pacific. Units: #/month.

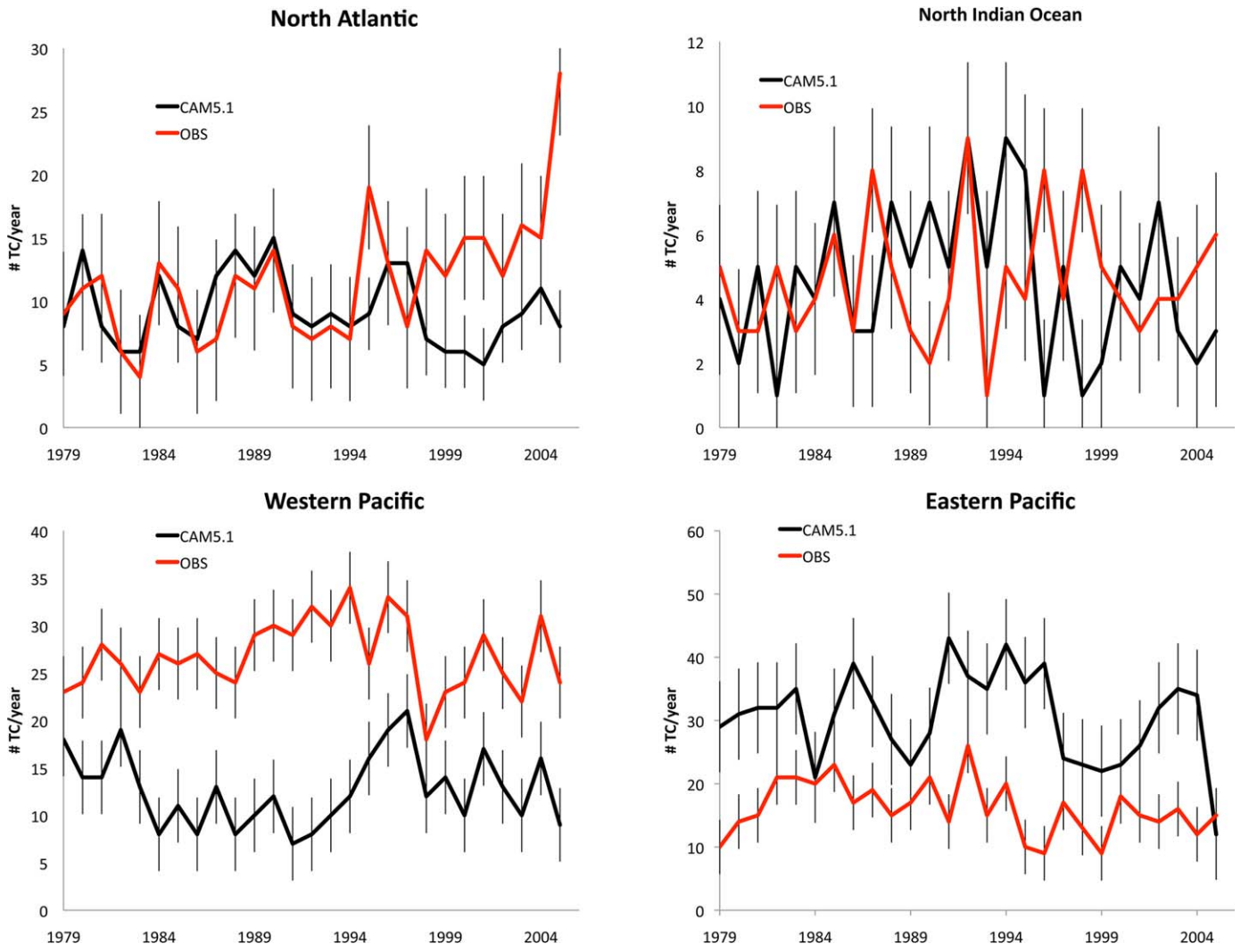

Figure 7. Annual counts of simulated (black) and observed (red) tropical storms over 1979–2005 in selected ocean basins for the high-resolution CAM5.1. (top right) North Atlantic. (top left) North Indian. (bottom left) West Pacific. (bottom right) East Pacific. Error bars are the interannual standard deviations. Units: #/yr.

One such example is in the North Atlantic basin from 1979 to 1994, the centered correlation between observed and modeled storm counts is 0.75. After 1994, as seen in the top left plot of Figure 7, the two time series are slightly anticorrelated resulting in essentially no correlation over the entire 1979–2005 integration period. Conversely, in the Northwest Pacific Basin, during the period 1979–1994, observations and models are anticorrelated but from 1994 to 2005 this correlation is suggesting that the influence of SST pattern is strong in this basin during the later part of the integration. Past work has demonstrated that interannual variations in tropical cyclone counts in global atmosphere models are sensitive to the SST patterns that exist in the lower boundary condition forcing [*Zhao et al.*, 2009]. However, due to high computational costs for the high-resolution simulation, the lack of a multimember ensemble makes it difficult to demonstrate statistical significance of the CAM5.1 representation of interannual variability in storm counts for individual basins. These limitations make it difficult to compare to the interannual variability demonstrated in similar studies, including *Zhao et al.* [2009]. Qualitatively, these examples illustrate the need to integrate climate models over at least multidecadal periods before robust conclusions can be drawn, and that ensemble simulations are needed at these high resolutions.

4. Computational Issues and Lessons Learned

Experience with high-resolution climate models such as described in this paper is limited and some current production practices require modification. The AMIP simulations were performed on hopper.nersc.gov, a

CRAY XE-6 at the National Energy Research Supercomputing Center. The total number of processing cores required for the highest resolution case was 7680 using both the Message Passing Interface (MPI) and Open Multi-Processing (OpenMP) interprocessor communication protocols. This was obtained by assigning 6 OpenMP threads to 1280 MPI tasks. Domain decomposition enabled by MPI alternates between a latitude-height and a latitude-longitude configuration [*Mirin and Sawyer*, 2005]. Typically, a simulated year required a wall-clock day to execute on this system. Delays waiting in queue effectively doubled the total turnaround time.

The entire output of the high-resolution simulation was just over 100TB. By using the parallel output capabilities of CESM, the execution time spent during the output phase of the simulation was kept to about 10% of the total. We assigned output tasks to only 39 of the 7680 processors. This number was arrived at by trial and error but is dependent on details of the computational system. It is possible that the time spent performing output tasks could be further reduced.

The CAM allows the output of a large variety of both time averaged and instantaneous fields at multiple frequencies. We saved data at monthly, daily, and three hourly intervals. Typically, users save all the variables at a given frequency in one set of files. However, because of the large data volumes in the present integrations, we learned that this may cause serious delays in the analysis of the simulation output. Rather, we recommend that the highest frequency of output be divided into multiple sets of output files according to their end uses. Thus, far less data are required to be staged from archival storage to the analysis platforms. For instance, in future simulations, we will save the data necessary for tropical storm tracking in a single set of files apart from the data necessary for driving regional model simulation even though they may be saved at the same frequency. Duplication of some output variables is cost effective in the long run by the time saved in the analysis stage of the simulation.

5. Conclusions

We present a detailed analysis of the performance of CAM5.1 as a function of horizontal resolution ranging from ∼200 to ∼25 km at the equator. We find that the ability of the model to reproduce observations of the recent past atmospheric state is mixed as resolution increases. While the simulated weather at high resolution offers more realism in terms of reproducing intense storms and in some mean fields that are strongly influenced by local orography, mean fields at large scales are often better represented by the tuned ∼100 km public release version of the model than by the high-resolution simulation presented here.

Midlatitude winter and spring extreme precipitation over land are significantly better represented in the high-resolution model configuration. However, midlatitude summer extreme precipitation over land is significantly too large in the high-resolution model configuration, perhaps coincidentally similar to several of the NARCCAP regional models. This bias may be a result of the inherent spatial and temporal scales of the cumulus convection parameterization used in CAM5.1. In particular, a reduction in the "physics" time step imposed to keep the ratio of physics to dynamics operations constant is incommensurate with the default 1 h relaxation time scale of the CAM5.1 Zhang-McFarlane convection scheme [*Williamson*, 2013]. Land to atmosphere interactions also may play a role in this seasonal bias, as such phenomena are larger in warmer regions. We intend to examine these issues in future high-resolution simulations.

Little or no convergence of extreme precipitation statistics is exhibited at the resolutions presented in this study. However, the simulations here do exhibit some quantitative measures of improvement. While we find little improvement in the skill of the high-resolution model over the coarser released version of CAM5.1 in a fairly broad survey of mean fields, we do find that skill in simulating two measures of extreme precipitation are substantially improved outside of the warm regions of the planet when judged against available gridded observational daily data sets. The annual maximum of the 5 day accumulated precipitation is a measure of total extreme storm intensities and is found to be substantially larger over the wetter land regions in the high-resolution simulation and in better agreement with observations than are the low-resolution simulations. Similarly, 20 year seasonal return values of the seasonal maximum daily precipitation are also larger in the high-resolution simulation with acceptable agreement with observations in many land areas and seasons where cumulus processes do not provide significant contributions to total precipitation. However, significant inconsistencies between the various observational products temper these apparent improvements and an expert review of them would be of great value to model developers and analysts in the design of new parameterizations and the assessment of their influence on simulated extreme precipitation. A weakness of the standard performance measures presented in the paper is their inability to capture changes in fine-scale

spatial details as resolution is increased. The need for improved measures that do not simply average out these details is critical to assessing the performance of high-resolution atmospheric.

Tropical storm statistics are well reproduced by the ~25 km version of CAM5.1 with storms simulated up to category 5 on the Saffir-Simpson scale. Global tropical storm annual frequency is well characterized, as is the annual cycle at the basin scale. The most significant bias is a tendency for too many simulated tropical storms in the North Central Pacific, leading to too few storms propagating into the Western Pacific. Observed interannual variability is not well reproduced at the basin scale. However, the observed relationship between minimum central storm pressures and maximum wind speed is well reproduced by the high-resolution model.

Increasing resolution will not improve those aspects of a climate model simulation that are deficient because of poorly parameterized processes. Our analysis revealed that many of the large-scale mean biases (such as the tendency to form a "double ITCZ") in CAM5.1 are not improved by increased model fidelity and may in fact be made significantly worse. However, better representation of orography does lead to improvement of localized mean climatic features in many land regions. Furthermore, the enhanced realism of simulated storms through higher precipitation rates, stronger winds, and sharper gradients permits new classes of analyses of extreme weather in a changing climate. Execution of a multidecadal simulation at ~25 km has proved challenging but possible using an advanced high-performance computing facility. We are confident that such calculations will become routine in the not too distant future leading to enhanced understanding of future changes to extreme weather as the global climate warms.

Appendix A: Details of CAM5.1

The version of the Community Atmospheric Model (CAM5.1) employed in this study uses a mass conserving finite-volume (FV) dynamical core built on a shallow water approach in the horizontal direction [*Lin*, 2004]. The vertical discretization follows a Lagrangian control-volume principle based upon a terrain-following Lagrangian coordinate system and a fixed Eulerian reference frame. In particular, the vertically stacked volumes are allowed to shift along the local radial direction for several subcycled dynamical time steps before the horizontal faces of each volume are mapped back to fixed reference levels. The advection algorithm makes use of the monotonic Piecewise Parabolic Method with an explicit time stepping scheme [*Lin and Rood*, 1996]. A regular latitude-longitude computational mesh is selected that includes both pole points and is filtered to damp computational modes arising from violations of the Courant stability criterion. The prognostic variables are staggered on an Arakawa-D grid.

The CAM5.1 physical parameterization package uses the *Zhang and McFarlane* [1995] deep convective parameterization and the University of Washington (UW) shallow convection scheme [*Park and Bretherton*, 2009]. The convective parameterization includes a dilute entraining plume [*Neale et al*., 2008] and a convective momentum transport approximation as used in the previous version of the model, CAM4 [*Richter and Rasch*, 2008]. The moist boundary layer turbulence scheme is that of *Bretherton and Park* [2009]. A description of the surface flux parameterizations, an important driver for tropical cyclogenesis, is described in *Neale et al*. [2010].

In addition, parameterizations of cloud microphysics, cloud macrophysics, orographic gravity wave drag, the radiative effects of aerosols, and parameterizations of shortwave and longwave radiations are included [*Neale et al*., 2010]. The version of CAM5.1 used in this particular study used a so-called bulk aerosol model with prescribed rather than prognostic aerosols in order to reduce computational costs. The prescribed sea surface temperatures and sea ice concentrations are based on the standard CAM5 release data sets [*Hurrell et al*., 2008]. Differences among select parameters employed for the three resolutions required by tuning and stability considerations are listed in Table A1.

Table A1. The Stability and Tuning Parameters That Were Varied in This Study[a]

	CAM5.1 Namelist Variable	1.9° × 2.6°	0.9° × 1.3°	0.23° × 0.31°
Physics time step	dtime	1800 s	1800 s	900 s
Number of dynamics cycles per physics cycle	nsplit	4	8	18
Dynamics time step	= dtime/nsplit	450 s	225 s	50 s
Penetrative entrainment efficiency	uwshcu_rpen	5	10	10
Minimum relative humidity for low stable clouds	cldfrc_rhminl	0.8875D0	0.8975D0	0.8975D0

[a]All other input parameters were set to the values in public release version of the 0.9° × 1.3° configuration.

Appendix B

Table B1 shows a summary of global and basin scale observed and simulated tropical storm statistics to document future changes to the Community Atmospheric Model and for comparison to similar high-resolution models. Basins are defined in Table B2.

Table B1. Comparison of Annually Average Tropical Storm Statistics Between the 0.23° × 0.31° CAM5.1 and Emanuel Tracks Over the Period 1979–2005[a]

	Global	North Atlantic	East Pacific	West Pacific	North Indian	South Indian	Australia	South Pacific
Observed								
TS/yr	85.1 ± 9.6	11.6 ± 4.9	16.1 ± 4.3	26.8 ± 3.8	4.6 ± 1.9	11.6 ± 2.8	8.7 ± 3.6	5.7 ± 3.7
TC/yr	47.9 ± 6.9	6.5 ± 3.0	9.0 ± 3.0	17.3 ± 3.6	1.3 ± 1.2	6.1 ± 2.5	4.3 ± 2.1	3.3 ± 2.7
Intense TC/yr	14.9 ± 5.7	1.6 ± 1.5	2.7 ± 2.0	6.7 ± 2.8	0.3 ± 0.6	1.6 ± 1.3	1.1 ± 1.4	0.8 ± 1.1
TS days/yr	428.7 ± 69.5	65.5 ± 34.4	73.9 ± 28.9	149.5 ± 41.1	13.3 ± 6.5	60.8 ± 22.0	39.5 ± 15.9	26.3 ± 20.6
TC days/yr	175.2 ± 34.5	25.2 ± 16.3	31.3 ± 15.1	71.4 ± 23.0	2.6 ± 2.4	21.8 ± 11.0	12.8 ± 7.0	10.2 ± 9.5
Intense TC days/yr	28.0 ± 14.4	3.3 ± 3.9	3.9 ± 3.2	14.6 ± 8.8	0.3 ± 0.6	2.8 ± 2.8	1.6 ± 2.3	1.5 ± 2.2
0.23° × 0.31° CAM5.1								
TS/yr	82.6 ± 8.8	9.3 ± 2.9	30.5 ± 7.2	12.7 ± 3.9	4.5 ± 2.4	13.4 ± 4.4	8.0 ± 2.8	4.0 ± 2.7
TC/yr	51.7 ± 7.2	7.1 ± 3.2	18.4 ± 6.0	8.3 ± 2.9	2.4 + 1.6	7.8 ± 2.8	5.0 ± 1.7	2.5 ± 2.0
Intense TC/yr	8.9 ± 2.7	1.8 ± 1.6	2.3 ± 1.9	2.8 ± 1.5	0.2 ± 0.4	1.1 ± 1.1	0.4 ± 0.6	0.1 ± 0.4
TS days/yr	840.4 ± 102.3	99.5 ± 35.8	262.5 ± 69.3	189.9 ± 52.6	45.0 ± 20.8	145.2 ± 45.4	64.9 ± 23.9	31.6 ± 22.2
TC days/yr	222.9 ± 49.8	39.6 ± 19.6	60.3 ± 27.9	66.3 ± 28.1	5.1 ± 4.1	31.8 ± 13.4	12.8 ± 6.8	6.5 ± 7.5
Intense TC days/yr	16.7 ± 8.5	3.4 ± 4.2	0.9 ± 1.4	9.4 ± 6.7	0.1 ± 0.3	2.1 ± 2.2	0.7 ± 1.2	0.1 ±0.6

[a]Mean values and their interannual standard deviations are shown for the entire globe and individually for storms originating in the individual ocean basins. Regions are as defined in Table B2.

Table B2. Definition of Ocean Basin Longitude Boundaries for Data Binning in Table B1[a]

Basin	Longitude Minimum	Longitude Maximum
North Indian	40	105
West Pacific	105	200
East Pacific	200	Variable
North Atlantic	Variable	340
South Indian	30	105
Australia	105	165
South Pacific	165	265

[a]The latitudinal boundary is defined to be the equator and respective pole. Note that the boundary between the East Pacific and North Atlantic basins is variable, following the general shape of Central America.

Acknowledgments

This work was supported by the Regional and Global Climate Modeling Program of the Office of Biological and Environmental Research in the U.S. Department of Energy Office of Science under contract DE-AC02–05CH11231. K. R. Sperber and P. J. Gleckler were supported by the Office of Science (BER), U.S. Department of Energy through Lawrence Livermore National Laboratory contract DE-AC52-07NA27344. C. Jablonowski was supported by the U.S. Department of Energy's SciDAC program, grant DE-SC0006684. Calculations were performed at the National Energy Research Supercomputing Center (NERSC) at the Lawrence Berkeley National Laboratory where the data from these simulations are archived and available from the authors. This document was prepared as an account of work sponsored by the U.S. Government. While this document is believed to contain correct information, neither the U.S. Government nor any agency thereof, nor the Regents of the University of California, nor any of their employees, makes any warranty, express or implied, or assumes any legal responsibility for the accuracy, completeness, or usefulness of any information, apparatus, product, or process disclosed, or represents that its use would not infringe privately owned rights. Reference herein to any specific commercial product, process, or service by its trade name, trademark, manufacturer, or otherwise, does not necessarily constitute or imply its endorsement, recommendation, or favoring by the U.S. Government or any agency thereof, or the Regents of the University of California. The views and opinions of authors expressed herein do not necessarily state or reflect those of the U.S. Government or any agency thereof or the Regents of the University of California.

References

Adam, J. C., and D. P. Lettenmaier (2003), Adjustment of global gridded precipitation for systematic bias, *J. Geophys. Res.*, *108*(D9), 4257, doi:10.1029/2002JD002499.

Alexander, L. V., et al. (2006), Global observed changes in daily climate extremes of temperature and precipitation, *J. Geophys. Res.*, *111*, D05109, doi:10.1029/2005JD006290.

Arakawa, A., and C.-M. Wu (2013), A unified representation of deep moist convection in numerical modeling of the atmosphere: Part I, *J. Atmos. Sci.*, *70*, 1977–1992, doi: http://dx.doi.org/10.1175/JAS-D-12-0330.1.

Atlas, R., O. Reale, B.-W. Shen, S.-J. Lin, J.-D. Chern, W. Putman, T. Lee, K.-S. Yeh, M. Bosilovich, and J. Radakovich (2005), Hurricane forecasting with the high-resolution NASA finite volume general circulation model, *Geophys. Res. Lett.*, *32*, L03807, doi:10.1029/2004GL021513.

Bacmeister, J. T., M. Wehner, R. B. Neale, A. Gettelman, C. Hannay, P. Lauritzen, and J. Caron (2013), Exploratory high-resolution climate simulations using the Community Atmosphere Model (CAM), *J. Clim.*, *27*, 3073–3099, doi:10.1175/jcli-d-13-00387.1.

Bengtsson, L., K. I. Hodges, M. Esch, N. Keenlyside, L. Kornblueh, J. Luo, and T. Yamagata (2007), How many tropical cyclones change in a warmer climate?, *Tellus, Ser. A*, *59*, 539–561, doi:10.1111/j.1600-0870.2007.00251.x.

Bolvin, D. T., R. F. Adler, G. J. Huffman, E. J. Nelkin, and J. P. Poutiainen (2009), Comparison of GPCP monthly and daily precipitation estimates with high-latitude gauge observations, *J. Appl. Meteorol. Climatol.*, *48*, 1843–1857.

Boyle, J., and S. A. Klein (2010), Impact of model horizontal resolution on climate model forecasts of tropical precipitation and diabatic heating for the TWP-ICE period, *J. Geophys. Res.*, *115*, D23113, doi:10.1029/2010JD014262.

Bretherton, C. S., and S. Park (2009), A new moist turbulence parameterization in the Community Atmosphere Model, *J. Clim.*, *22*, 3422–3448, doi:10.1175/2008JCLI2556.1.

Camargo, S., and A. Sobel (2010), Revisiting the influence of the quasi-biennial oscillation on tropical cyclone activity, *J. Clim.*, *23*, 5810–5825.

Camargo, S., A. Sobel, A. Barnston, and P. Klotzbach (2010), The influence of natural climate variability, and seasonal forecasts of tropical cyclone activity, in *Global Perspectives on Tropical Cyclones*, 2nd ed., edited by J. C. L. Chan and J. D. Kepert, pp. 325–360, World Scientific Publishing Co., Singapore.

Chen, J.-H., and S.-J. Lin (2011), The remarkable predictability of inter-annual variability of Atlantic hurricanes during the past decade, *Geophys. Res. Lett.*, *38*, L11804, doi:10.1029/2011GL047629.
Coles, S. (2001), *An Introduction to Statistical Modeling of Extreme Values*, Springer, London.
Covey, C., K. M. AcutaRao, M. Fiorino, P. J. Gleckler, K. E. Taylor, and M. F. Wehner (2002), Intercomparison of climate data sets as a measure of observational uncertainty, *PCMDI Rep. 69, LLNL Rep. UCRL-ID-147371*, Lawrence Livermore National Laboratory, Livermore, Calif.
Donat, M. G., L. V. Alexander, H. Yang, I. Durre, R. Vose, and J. Caesar (2013), Global land-based datasets for monitoring climatic extremes, *Bull. Am. Meteorol. Soc.*, *94*, 997–1006.
Donner, L. J., et al. (2011), The dynamical core, physical parameterizations, and basic simulation characteristics of the atmospheric component AM3 of the GFDL global coupled model CM3, *J. Clim.*, *24*, 3484–3519, doi:10.1175/2011JCLI3955.1.
Duffy, P. B., B. Govindasamy, J. Milovich, K. Taylor, M. Wehner, A. Lamont, and S. Thompson (2003), High resolution simulations of global climate, Part 1: Present climate, *Clim. Dyn.*, *21*, 371–290.
Emanuel, K. (2007), Environmental factors affecting tropical cyclone power dissipation, *J. Clim.*, *20*, 5497–5509.
Emanuel, K. A. (2005), Increasing destructiveness of tropical cyclones over the past 30 years, *Nature*, *436*, 686–688.
Frich, P., L. V. Alexander, P. Della-Marta, B. Gleason, M. Haylock, A. M. G. Klein Tank, and T. Peterson (2002), Observed coherent changes in climate extremes during the second half of the twentieth century, *Clim. Res.*, *19*, 193–212.
Fudeyasu, H., Y. Wang, M. Satoh, T. Nasuno, H. Miura, and W. Yanase (2008), Global cloud-system-resolving model NICAM successfully simulated the lifecycles of two real tropical cyclones, *Geophys. Res. Lett.*, *35*, L22808, doi:10.1029/2008GL036003.
Gates, W. L. (1992), AMIP: The Atmospheric Model Intercomparison Project, *Bull. Am. Meteorol. Soc.*, *73*, 1962–1970.
Gates, W. L., et al. (1999), An overview of the results of the Atmospheric Model Intercomparison Project (AMIP I), *Bull. Am. Meteorol. Soc.*, *80*, 29–55.
Gettelman, A., H. Morrison, and S. J. Ghan (2008), A new two-moment bulk stratiform cloud microphysics scheme in the Community Atmospheric Model (CAM3), Part II: Single-column and global results, *J. Clim.*, *21*, 3660–3679.
Ghan, S. J., X. Liu, R. C. Easter, R. Zaveri, P. J. Rasch, J.-H. Yoon, and B. Eaton (2012), Toward a minimal representation of aerosols in climate models: Comparative decomposition of aerosol direct, semidirect, and indirect radiative forcing, *J. Clim.*, *25*, 6461–6476.
Haylock, M. R., N. Hofstra, A. M. G. Klein Tank, E. J. Klok, P. D. Jones, and M. New (2008), A European daily high-resolution gridded dataset of surface temperature and precipitation, *J. Geophys. Res.*, *113*, D20119, doi:10.1029/2008JD010201.
Higgins, R. W., W. Shi, E. Yarosh, and R. Joyce (2000), Improved United States precipitation quality control system and analysis, *NCEP/Clim. Predict. Cent. ATLAS 7*, 40 pp., National Centers for Environmental Prediction, National Oceanic and Atmospheric Administration, US Department of Commerce, Camp Springs, Md.
Huffman, G. J., R. F. Adler, M. M. Morrissey, S. Curtis, R. Joyce, B. McGavock, and J. Susskind (2001), Global precipitation at one-degree daily resolution from multi-satellite observations, *J. Hydrometeorol.*, *2*, 36–50.
Huffman, G. J., R. F. Adler, D. T. Bolvin, G. Gu, E. J. Nelkin, K. P. Bowman, Y. Hong, E. F. Stocker, and D. B. Wolff (2007), The TRMM multi-satellite precipitation analysis: Quasi-global, multi-year, combined-sensor precipitation estimates at fine scale, *J. Hydrometeorol.*, *8*, 38–55.
Hurrell, J. W., J. J. Hack, D. Shea, J. M. Caron, and J. Rosinski (2008), A new sea surface temperature and sea ice boundary dataset for the community atmosphere model, *J. Clim.*, *21*(19), 5145–5153.
Karl, T. R., J. M. Melillo, and T. C. Peterson (2009), *Global Climate Change Impacts in the United States*, Cambridge Univ. Press, New York.
Kharin, V.V., F.W. Zwiers, X. Zhang, and G.C. Hegerl (2007), Changes in temperature and precipitation extremes in the IPCC ensemble of global coupled model simulations, *J. Clim.*, *20*, 1419–1444.
Kharin, V. V., F. W. Zwiers, X. Zhang, and M. Wehner (2013), Changes in temperature and precipitation extremes in the CMIP5 ensemble, *Clim. Change*, *119*, 345–357, doi:10.1007/s10584-013-0705-8.
Knapp, K. R., M. C. Kruk, D. H. Levinson, H. J. Diamond, and C. J. Neumann (2010), The International Best Track Archive for Climate Stewardship (IBTrACS): Unifying tropical cyclone best track data, *Bull. Am. Meteorol. Soc.*, *91*, 363–376, doi:10.1175/2009BAMS2755.1.
Knutson, T. R., J. J. Sirutis, S. T. Garner, I. Held, and R. E. Tuleya (2007), Simulation of the recent multidecadal increase of Atlantic hurricane activity using an 18-km-grid regional model, *Bull. Am. Meteorol. Soc.*, *88*, 1549–1565, doi:10.1175/BAMS-88-10-1549.
Knutson, T. R., I. Held, J. L. McBride, J. Chan, K. Emanuel, G. Holland, C. Landsea, J. P. Kossin, A. K. Srivastava, and M. Sugi (2010), Tropical cyclones and climate change, *Nat. Geosci.*, *3*, 157–163.
Landsea, C. W., G. A. Vecchi, L. Bengtsson, and T. R. Knutson (2010), Impact of duration thresholds on Atlantic Tropical cyclone counts, *J. Clim.*, *23*, 2508–2519.
Li, F., W. D. Collins, M. F. Wehner, D. Williamson, J. Olson, and C. Algieri (2011), Impact of horizontal resolution on simulation of precipitation extremes in an aqua-planet version of Community Atmospheric Model (CAM3), *Tellus, Ser. A*, *63*, 884–823.
Lin, S.-J. (2004), A "vertically Lagrangian" finite-volume dynamical core for global models, *Mon. Weather Rev.*, *132*, 2293–2307.
Lin, S.-J., and R. B. Rood (1996), Multidimensional flux-form semi-Lagrangian transport scheme, *Mon. Weather Rev.*, *124*, 2046–2070.
Maurer, E. P., A. W. Wood, J. C. Adam, D. P. Lettenmaier, and B. Nijssen (2002), A long-term hydrologically-based data set of land surface fluxes and states for the conterminous United States, *J. Clim.*, *15*, 3237–3251.
Maurer, E. P., J. C. Adam, and A. W. Wood (2009), Climate model based consensus on the hydrologic impacts of climate change to the Rio Lempa basin of Central America, *Hydrol. Earth Syst. Sci.*, *13*, 183–194.
McClean, J. L., et al. (2011), A prototype two-decade fully-coupled fine-resolution CCSM simulation, *Ocean Modell.*, *39*, 10–30, doi:10.1016/j.ocemod.2011.02.011.
Mearns, L. O., W. J. Gutowski, R. Jones, L.-Y. Leung, S. McGinnis, A. M. B. Nunes, and Y. Qian (2009), A regional climate change assessment program for North America, *EOS*, *90*, 311–312.
Melillo, J. M. , Terese (T.C.) Richmond, and G. W. Yohe, eds., (2014), *Climate Change Impacts in the United States: The Third National Climate Assessment*. *U.S. Global Change Research Program*, Washington, DC, 841 pp., doi:10.7930/J0Z31WJ2.
Mirin, A. A., and W. B. Sawyer (2005), A scalable implementation of a finite-volume dynamical core in the community atmospheric model, *Int. J. High Performence Comput. Appl.*, *19*, 203–212.
Neale, R. B., J. H. Richter, and M. Jochum (2008), The impact of convection on ENSO: From a delayed oscillator to a series of events, *J. Clim.*, *21*, 5904–5924, doi:10.1175/2008JCLI2244.1.
Neale, R. B., et al. (2010), Description of the NCAR Community Atmosphere Model (CAM 5.0), *NCAR Tech. Note NCAR/TN-486+STR*, 282 pp., Natl. Cent. for Atmos. Res., Boulder, Colo.
Oouchi, K., J. Yoshimura, H. Yoshimura, R. Mizuta, S. Kusonoki, and A. Noda (2006), Tropical cyclone climatology in a global-warming climate as simulated in a 20 km-mesh global atmospheric model: Frequency and wind intensity analyses, *J. Meteorol. Soc. Jpn.*, *84*(2), 259–276.

Park, S., and C. S. Bretherton (2009), The University of Washington shallow convection and moist turbulence schemes and their impact on climate simulations with the Community Atmosphere Model, *J. Clim.*, *22*, 3449–3469, doi:10.1175/2008JCLI2557.1.

Prabhat, O. Ruebel, S. Byna, K. Wu, F. Li, M. Wehner, and W. Bethel (2012), TECA: A Parallel Toolkit for Extreme Climate Analysis, International Conference on Computational Science, ICCS 2012, Workshop on Data Mining in Earth System Science, *Procedia Computer Science*.

Reed, K. A., and C. Jablonowski (2011a), An analytic vortex initialization technique for idealized tropical cyclone studies in AGCMs, *Mon. Weather Rev.*, *139*, 689–710, doi:10.1175/2010MWR3488.1.

Reed, K. A., and C. Jablonowski (2011b), Assessing the uncertainty of tropical cyclone simulations in NCAR's Community Atmosphere Model, *J. Adv. Model. Earth Syst.*, *3*, M08002, doi:10.1029/2011MS000076.

Reed, K. A., and C. Jablonowski (2012), Idealized tropical cyclone simulations of intermediate complexity: A test case for AGCMs, *J. Adv. Model. Earth Syst.*, *4*, M04001, doi:10.1029/2011MS000099.

Richter, J. H., and P. J. Rasch (2008), Effects of convective momentum transport on the atmospheric circulation in the Community Atmosphere Model, version 3, *J. Clim.*, *21*, 1487–1499, doi:10.1175/2007JCLI1789.1.

Seneviratne, S. I., et al. (2012), Changes in climate extremes and their impacts on the natural physical environment, in *Managing the Risks of Extreme Events and Disasters to Advance Climate Change Adaptation. A Special Report of Working Groups I and II of the Intergovernmental Panel on Climate Change (IPCC)*, edited by C. B. Field et al., pp. 109–230, Cambridge Univ. Press, New York.

Shen, B.-W., R. Atlas, J.-D. Chern, O. Reale, S.-J. Lin, T. Lee, and J. Chang (2006a), The 0.125 degree finite-volume general circulation model on the NASA Columbia supercomputer: Preliminary simulations of mesoscale vortices, *Geophys. Res. Lett.*, *33*, L05801, doi:10.1029/2005GL024594.

Shen, B.-W., R. Atlas, O. Reale, S.-J. Lin, J.-D. Chern, J. Chang, C. Henze, and J.-L. Li (2006b), Hurricane forecasts with a global mesoscale-resolving model: Preliminary results with hurricane Katrina (2005), *Geophys. Res. Lett.*, *33*, L13813, doi:10.1029/2006GL026143.

Stocker, T.F., D. Qin, G.-K. Plattner, M. Tignor, S.K. Allen, J. Boschung, A. Nauels, Y. Xia, V. Bex, and P.M. Midgley, eds., (2013), *IPCC, 2013: Climate Change 2013: The Physical Science Basis. Contribution of Working Group I to the Fifth Assessment Report of the Intergovernmental Panel on Climate Change*, 1535 pp, Cambridge Univ. Press, Cambridge, U. K. and New York.

Strachan, J., P. L. Vidale, K. Hodges, M. Roberts, and M.-E. Demory (2013), Investigating global tropical cyclone activity with a hierarchy of AGCMs: The role of model resolution, *J. Clim.*, *26*, 133–152.

Sugi, M., H. Murakami, and J. Yoshimura (2009), A reduction in global tropical cyclone frequency due to global warming, *Sci. Online Lett. Atmos.*, *5*, 164–167.

Taylor, K. E. (2001), Summarizing multiple aspects of model performance in single diagram, *J. Geophys. Res.*, *106*, 7183–7192.

Tomita, H., and M. Satoh (2004), A new dynamical framework of non-hydrostatic global model using the icosahedral grid, *Fluid Dyn. Res.*, *34*, 357–400.

Wehner, M. F. (2012), Very extreme seasonal precipitation in the NARCCAP ensemble: Model performance and projections, *Clim. Dyn.*, *40*, 59–80, doi:10.1007/s00382-012-1393-1.

Wehner, M. F., G. Bala, P. Duffy, A. A. Mirin, and R. Romano (2010a), Towards direct simulation of future tropical cyclone statistics in a high-resolution global atmospheric model, *Adv. Meteorol.*, *0102*, 915303, doi:10.1155/2010/915303.

Wehner, M. F., R. Smith, P. Duffy, and G. Bala (2010b), The effect of horizontal resolution on simulation of very extreme US precipitation events in a global atmosphere model, *Clim. Dyn.*, *32*, 241–247, doi:10.1007/s00382009-0656-y.

Williamson, D. L. (2013), The effect of time steps and time-scales on parameterization suites, *Q. J. R. Meteorol. Soc.*, *139*, 548–560.

Yamada, Y., K. Oouchi, M. Satoh, H. Tomita, and W. Yanase (2010), Projection of changes in tropical cyclone activity and cloud height due to greenhouse warming: Global cloud-system-resolving approach, *Geophys. Res. Lett.*, *37*, L07709, doi:10.1029/2010GL042518.

Yatagai, A., K. Kamiguchi, O. Arakawa, A. Hamada, N. Yasutomi, and A. Kitoh (2012), APHRODITE: Constructing a long-term daily gridded precipitation dataset for Asia based on a dense network of rain gauges, *Bull. Am. Meteorol. Soc.*, *93*, 1401–1415, doi:10.1175/BAMS-D-11-00122.1.

Yoshimura, J., and M. Sugi (2005), Tropical cyclone climatology in a high-resolution AGCM-impacts of SST warming and CO_2 increase, *Sci. Online Lett. Atmos.*, *1*, 133–136.

Zhang, G. J., and N. A. McFarlane (1995), Sensitivity of climate simulations to the parameterization of cumulus convection in the Canadian Climate Centre General Circulation Model, *Atmos. Ocean*, *33*, 407–446.

Zhao, M., I. M. Held, S.-J. Lin, and G. A. Vecchi (2009), Simulations of global hurricane climatology, interannual variability, and response to global warming using a 50-km resolution GCM, *J. Clim.*, *22*, 6653–6678.